Available online at www.sciencedirect.com
SCIENCE DIRECT®
Journal of Molecular Catalysis A: Chemical 222 (2004) 133–141
JOURNAL OF MOLECULAR CATALYSIS A: CHEMICAL
www.elsevier.com/locate/molcata

Catalytic degradation of expandable polystyrene waste (EPSW) over mordenite and modified mordenites

Vilas Ramdas Chumbhale[1], Jun-Sik Kim, Sang-Bong Lee, Myoung-Jae Choi*

Advanced Chemical Technology Division-ENR, KRICT, Taejon 305-600, Korea

Received 14 January 2004; received in revised form 29 June 2004; accepted 1 July 2004
Available online 13 September 2004

Abstract

The performance of the several different modified mordenite zeolites in the degradation of expandable polystyrene waste (EPSW) was investigated in this study. The composition of the degradation products, especially the liquid fraction was compared to understand the role of H-mordenite and the effect of its modification through framework dealumination and metal impregnation. The degradation was carried out in a batch reactor at 360 and 400 °C. The dealuminated mordenite with SiO_2/Al_2O_3 ratio of 86 showed enhanced styrene/styrene dimer and styrene/ethylbenzene molar ratios at lower (360 °C) and higher (400 °C) temperature, respectively. This was attributed to the intermediate acid strength distribution generated on removal of framework aluminum by acid leaching. Modification of H-mordenite by metal impregnation substantially changed the acidic and catalytic properties in polystyrene degradation. The 0.64 wt.% phosphorous loading on H-mordenite showed improved EPSW conversion, styrene yield and SM/EB molar ratio at 400 °C. The 0.32 wt.% phosphorous loading facilitated the improvement in SM/EB molar ratio with higher styrene selectivity than thermal degradation at 360 °C.

Keywords: Catalytic degradation; Modified mordenite; Dealumination; Polystyrene; Styrene selectivity

1. Introduction

The amount of waste plastic discarded each year is constantly increasing and is causing serious pollution problems. If this material can be chemically recycled, it will become a cheap and abundant source for useful chemicals and energy. Among various recycling methods, the chemical method which converts waste plastics to useful hydrocarbons, has been recognized as a promising approach [1,2].

Among the different solid acids, zeolites are the preferred catalysts for the conversion of plastic wastes [3]. Zeolite catalysts are extensively used in petroleum refinery and in petrochemical industry. Shape selectivity, tunable acidity and basicity, ion-exchange, isomorphous substitution and thermal stability are substantial properties of zeolite catalysts.

It is reported that medium pore zeolite HZSM-5 due to the presence of strong acid sites possesses potential for cleavage of C–C bonds in the waste plastics and can hydrogenate olefins, yielded by the degradation, into paraffins. Since olefins are easily oxidized or polymerized into unusable compounds during storage and transportation, oils containing a large fraction of olefins might not be suitable for fuel oils [4].

Mordenite is a one-dimensional wide pore zeolite having crystallographic pore size 6.7 Å × 7 Å interconnected with an eight-ring pore of 2.9 Å × 5.7 Å, one-dimensional. It exhibits orthorhombic symmetry with unit cell formula $Na_n[Al_nSi_{40-n}O_{96}]24H_2O$ [5]. It has proved to be a potential catalyst in hydrocarbon processing [6–8]. However, its use in the modified form is not much reported for polystyrene degradation. In the present work we have compared the utility of mordenite and its modified forms for title reaction.

* Corresponding author.
E-mail address: mjchoi@krict.re.kr (M.-J. Choi).
[1] Catalysis Division, National Chemical Laboratory, Pune 411008 (CSIR), India.

1381-1169/$ – see front matter © 2004 Published by Elsevier B.V.
doi:10.1016/j.molcata.2004.07.002

2. Experimental

2.1. Zeolite synthesis (Na mordenite)

Synthesis of sodium mordenite was carried out hydrothermally from system containing Na_2O–Al_2O_3–SiO_2–H_2O. 168.2 g of sodium silicate (27.2% SiO_2, 8.4% Na_2O, 64.4% H_2O) were diluted with 200 g of deionized water. An acidic aluminum sulphate solution was made by taking 12.6 g of salt [$Al_2(SO_4)_3 18H_2O$] in 226 g of deionized water. This solution was then slowly added under stirring to the previously prepared sodium silicate solution. The reaction mixture was further intensively stirred for 1 h. The resulting gel having pH = 11 ± 0.2 was then transferred to a stainless steel autoclave. The autoclave was kept in a static air oven at 120 °C. After the gel was crystallized for 96 h under static conditions, the crystallization process was terminated by quenching the autoclave to room temperature. The crystalline solid was separated from the liquid by suction filtration. It was then thoroughly washed with hot deionized water till free of sulphate ions and dried in an air oven at 120 °C for 8 h. This sample was further calcined in flowing air at 500 °C for 12 h in a static air furnace to obtain the Na form of zeolite. The catalytic active protonic form (HM) was obtained by repeated ion exchange with dilute solution of 5% ammonium nitrate (solution/zeolite ratio 15). The final product was filtered, dried (in air oven at 120 °C for 8 h) and calcined at 500 °C for 12 h in a flow of dry air. The unit cell composition of fully crystalline mordenite sample in its H form, determined by wet chemical/gravimetric methods and atomic absorption spectrometry, was $Na_{0.33}H_{6.11}[(AlO_2)_{6.44}(SiO_2)_{41.56}]18H_2O$.

The HM zeolite was treated with mineral acid (HCl) at 98 °C under reflux, washed with hot deionized water to free it from chloride ions and then dried at 120 °C for 12 h. The H-mordenite zeolites with higher SiO_2/Al_2O_3 ratios were obtained by treating HM with mineral acid as shown in Table 1.

2.2. Preparation of phosphorous modified mordenite (PHM)

These samples were prepared by impregnating HM zeolite with appropriate quantity of *ortho*-phosphoric acid in aqueous solution. The well homogenized slurry was slowly evaporated at 98 °C for 12 h. and calcined in a muffle furnace at 460 °C for 10 h to give the corresponding catalyst in the oxide form. All samples were equilibriated with water vapor before further characterization by placing them over saturated ammonium chloride solution for 24 h at 25 °C. The samples were named PHM (0.32), PHM (0.64) and PHM (1.0) where figures in parentheses indicated wt.% of phosphorous impregnated.

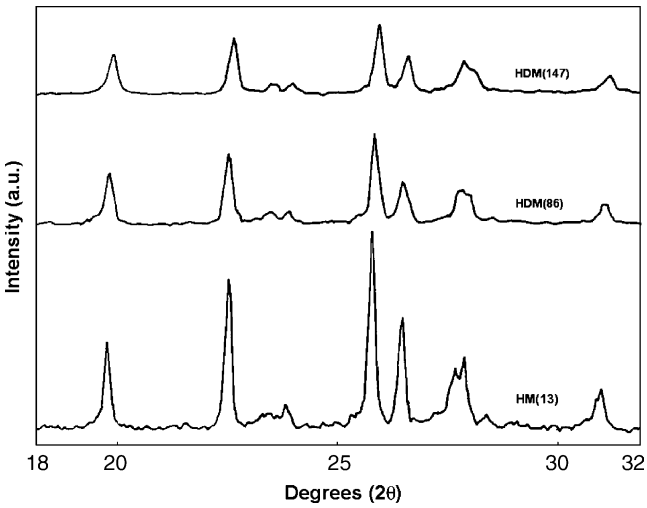

Fig. 1. XRD pattern of HM and HDM zeolites.

2.3. Characterization

Crystalline phase identification was done by recording XRD patterns on a Phillips diffractometer (PW-1730) using Cu Kα radiation (λ = 1.54014 Å). The samples were scanned in the 2θ range of 18–31. Fig. 1 depicts the XRD pattern of different mordenite samples. Sorption measurements were carried out in an all glass McBain–Baker type gravimetric apparatus using a silica spring (sensitivity = 50 cm/g) balance. Prior to sorption measurements, a 50 mg sample was activated at 400 °C for 4 h under vacuum (10^{-6} Torr). It was cooled to ambient temperature (25 °C) under vacuum and allowed to contact a sorbate vapor at P/P_0 = 0.5 and 0.8. Equilibrium sorption capacities were obtained over a period of 2 h. The data on sorption measurement is shown in Table 2.

The loss of aluminum from mordenite lattice by acid treatment was confirmed by ^{29}Si and ^{27}Al NMR. The solid state ^{29}Si and ^{27}Al MAS NMR spectra were recorded at

Table 1
Scheme of sample preparation by dealumination with mineral acid

Zeolite	Treatment	Unit cell composition	SiO_2/Al_2O_3 molar ratio
Na-M	–	$H_{1.2}Na_{6.84}[(SiO_2)_{39.97}(AlO_2)_{8.03}]$	9.96
HM (13)	–	$H_{5.84}Na_{0.46}[(SiO_2)_{41.76}(AlO_2)_{6.3}]$	13.26
HDM (86)	(a) 5N HCl boil 24 h (b) 5N HCl boil 24 h	$H_{0.97}Na_{0.12}[(SiO_2)_{46.91}(AlO_2)_{1.09}]$	86.0
HDM (147)	(a) 8N HCl boil 24 h (b) 8N HCl boil 24 h (c) 8.5N HCl boil 24 h	$H_{0.58}Na_{0.06}[(SiO_2)_{47.4}(AlO_2)_{0.64}]$	147

(b) Product of (a) was used for second treatment; (c) product of (b) was used for successive treatment.

Table 2
Equilibrium sorption data (molecules/u.c.) of HM and HDM zeolites

Zeolite	HM (13)	HDM (86)	HDM (147)
Water	35.04	27.62	23.50
n-Hexane	3.18	3.68	3.86
Cyclohexane	2.87	3.27	3.38
Benzene	4.08	4.15	4.34
Cumene	1.40	1.88	2.47

Sorption measurement at $P/P_0 = 0.5$ and at 25 °C.

ambient temperature using a Bruker MSL-300 FT-NMR spectrometer. Three thousand FIDs were accumulated before FT to get spectra with a good S/N ratio. A 5 s delay time was used for 90° pulse. TMS was used as the external reference for ^{29}Si signal. While an aqueous solution of $AlCl_3$ provided the reference peak for ^{27}Al, the spinning rate was kept at 3.5 kHz for all samples. Fig. 2(a) and (b) depict the ^{29}Si and ^{27}Al MAS NMR spectra for mordenite and dealuminated mordenite respectively.

The thermo-analytical curves (DTA, TG, DTG) of aluminum deficient mordenites were recorded using a thermal-analyzer under the following conditions: (1) sample weight 30 mg (2) heating rate 10 °C/min (3) sensitivity (DTA: 0.1 mV; DTG: 0.2 mV; TGA: 0–25 mg) (4) in the atmosphere of flowing air in the temperature range of 25–1000 °C and (5) α-alumina as a reference material. The TG curves of phosphorous impregnated mordenites (PHM) were recorded on a Setaram PC 92 thermal analyzer. For scanning the curves 30-35 mg sample was used in a platinum crucible, the heating rate being 10 °C/min and the temperature ranging from 25 to 1000 °C (α-alumina as a reference material). Fig. 3(a) and (b) depicts the TG curves of modified zeolites.

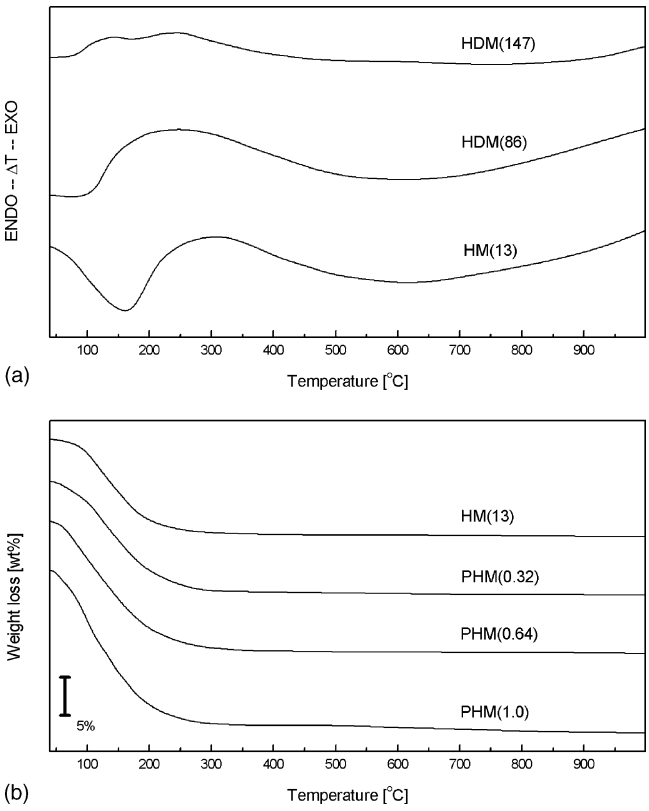

Fig. 3. TGA curves of HM, HDM and PHM zeolites.

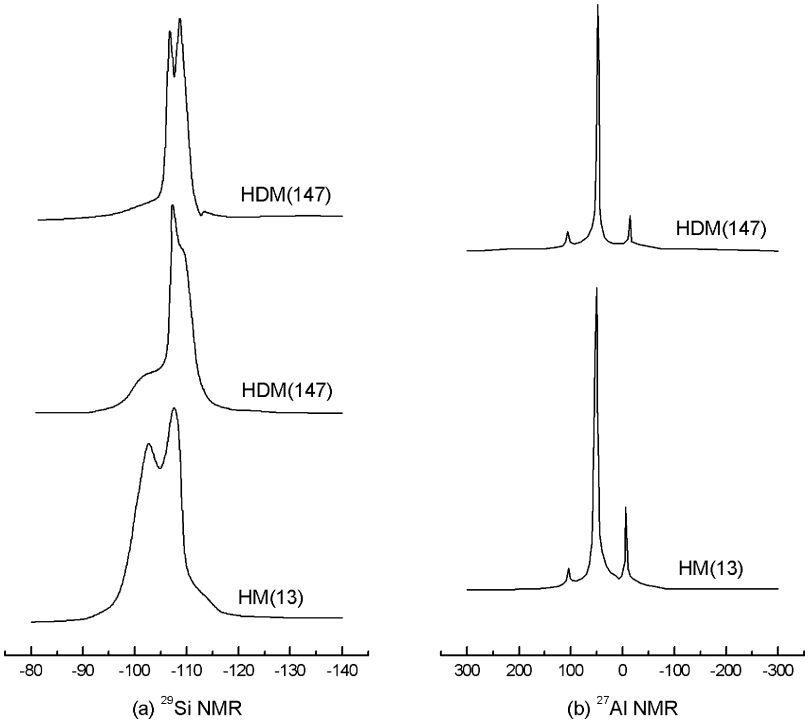

Fig. 2. ^{29}Si NMR and ^{27}Al NMR spectra of HM and HDM zeolites.

2.4. Acidity measurement (NH_3 TPD)

The total acidity of HM and modified mordenite was estimated by temperature programmed desorption (TPD) of NH_3. TPD measurements were done using a stainless steel micro-reactor connected on line to a gas chromatograph. In the typical experiment, 0.4 g of the zeolite sample (HM or HDM, 10–20 mesh size) was taken in a micro-reactor. It was initially heated to 400 °C at a rate of 10 °C/min in a flow of pure and dry nitrogen and then coupled to sorptiometer for evacuation. It was activated at 400 °C for 2 h and cooled to 150 °C. A calibrated volume of NH_3 having 99.8% purity was admitted to the sample which was further allowed to cool to 25 °C. The equilibrium adsorption of NH_3 was determined at 25 °C and 200 mmHg pressure. The loosely bound ammonia was evacuated at the same temperature. Equilibrium adsorption was once again determined at the same temperature and pressure. The difference between the ammonia adsorbed during the first and second determinations was taken as the chemisorbed ammonia. The micro-reactor was then coupled to the on-line GC after allowing sufficient time to stabilize the GC. The sample was heated at a linear rate of 10 °C/min with carrier gas flow rate of 60 ml/min. The total volume chemisorbed at 25 °C was obtained by volumetric measurements and the area % of desorption peaks are then used to calculate the acid strength distribution in the sample [9,10]. The TPD spectra of ammonia and the acidic properties of HM and HDM zeolites are shown in Fig. 4 and Table 3, respectively. The TPD profiles of PHM zeolites were recorded by adopting the same procedure (not shown here). Table 4 lists the acidity data of HM and PHM zeolites.

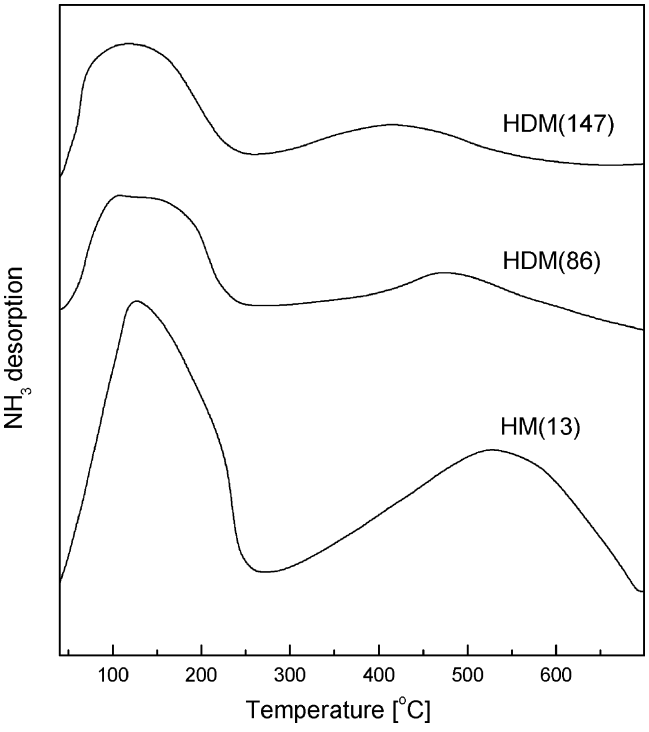

Fig. 4. NH_3 TPD profiles of HM and HDM zeolites.

Table 3
Acid sites distribution of HM and HDM zeolites

Zeolites	HM (13)	HDM (86)	HDM (147)
SiO_2/Al_2O_3	13	86	147
Al/u.c.	6.44	1.09	0.64
Acid sites/u.c. (weak + medium)	9.6	3.2	3.0
Acid sites/u.c. (stronger)	5.5	1.0	0.35
Acid sites/u.c. (total)	15.1	4.2	3.35
Stronger acid sites %	36.4	23.8	10.5
T_{max} (°C) (strong sites)	546	480	433

Table 4
Acidity data of HM and PHM zeolites

Zeolite[a]	Acid sites covered due to modifier species (mmol/g)	Acid sites covered due to modified species (%)	Accessible Al to NH_3 molecules[b] (mmol/g)
HM (13)	–	–	1.72
PHM (0.32)	0.28	16.28	1.44
PHM (0.64)	0.64	37.21	1.08
PHM (1.0)	0.86	50.0	0.86

[a] Figures in parentheses indicate percentage phosphorous impregnated.
[b] From TPD profile of respective sample.

2.5. EPSW degradation

2.5.1. Material

Expandable polystyrene waste having Mn = 100,100 and polydispersitivity index (Mw/Mn) = 2.2 was obtained from Korean agricultural and marine market. It was crushed and sieved into the range of 1–2 mm diameter prior to use in the reaction.

2.5.2. Reaction procedure

Both thermal and catalytic cracking experiments were carried out in a Pyrex batch reactor with an internal reactor volume of 250 ml. In a typical experiment, the catalyst was ground and sieved to get a particle size below 75 μm. EPS waste beads were ground and sieved to obtain a particle size below 1 mm. A mixture of 20 g of PS and the corresponding amount of catalyst (0.2 g) was loaded inside the reactor and heated with a rate of 10 °C/min up to 375 °C, kept at this temperature for 90 min. The reaction temperature was measured by thermocouples which were directly in contact with the reaction mixture. The volatile products were swept out from the reactor by a nitrogen stream and separated into gases and liquid oils in a condenser cooled by an ice-water mixture. The coke deposit on the reactor and catalyst was calculated by measuring the solid materials after extraction of residue using benzene as a solvent and filtration of extract carried out. The amount of gaseous products was calculated by subtracting the sum of weights for liquid, residues and catalyst with coke from total weight of EPSW sample and catalyst initially loaded to the reactor, except inorganic and metallic impurities [11]. The schematic of reaction set-up is showed in Fig. 5.

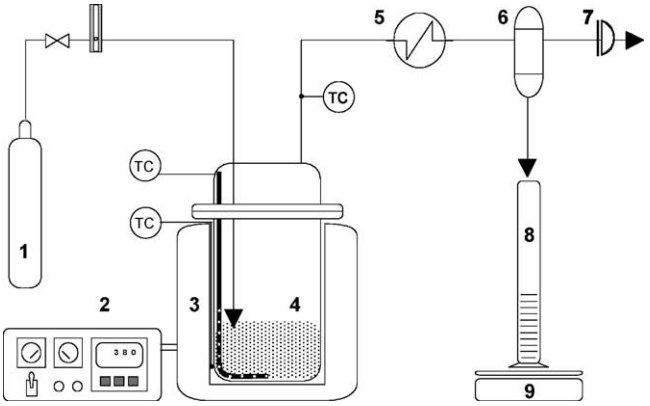

Fig. 5. Schematic of reactor assembly employed for EPSW degradation. (1) N_2 gas cylinder; (2) temperature controller; (3) electric heater; (4) batch reactor; (5) heat exchanger; (6) condenser; (7) wet gas meter; (8) receiver; (9) balance.

The conversion, selectivity and yield were calculated by employing following equations:

$$\text{PS conversion} = \text{liquid fraction (\%)} + \text{gas fraction (\%)} \quad (1)$$

$$\text{selectivity to specific (I) Product} = \frac{\text{specific product (I) in oil (g)}}{\text{liquid product (g)}} \times 100 \quad (2)$$

$$\text{SM yield (wt.\%)} = \frac{\text{SM obtained in oil (g)}}{\text{initial feed material (PS) taken (g)}} \times 100 \quad (3)$$

3. Results and discussion

3.1. Characterization of catalysts

From the XRD analysis of synthesized zeolite it was confirmed that the aluminosilicate had a mordenite structure [12,13]. The spectra of dealuminated and metal impregnated zeolite showed that there was no change in diffraction pattern and samples were well crystalline after modification by dealumination and metal impregnation. All samples were highly crystalline and were in the range of 95–98%. No evidence of lattice degradation was apparent in agreement with the previous report [14]. The X-ray diffraction patterns of phosphorous impregnated mordenites were found to be similar and products were well crystalline (spectra not shown here).

Fig. 2(a) shows the spectra of ^{29}Si MAS NMR of the HM and HDM zeolites. The spectrum of sample HM (13) showed two different peaks at −105 and −112 ppm which are assigned to Si (1Al) and Si (0Al) unit, respectively. The peak at −105 ppm arose not only from Si (1Al) but also from Si (OH) group [15]. After dealumination with HCl, HDM (86), the part of aluminum has been removed from the framework mordenite structure which has been clearly seen from the spectrum where Si (1Al) peak at −105 ppm decreased which is direct evidence of removal of aluminum from framework without disrupting the framework structure as is further confirmed by XRD pattern in the previous section. Further dealumination led to complete disappearance of peak at −105 ppm and fine crystallographic sites arose from the highly dealuminated sample with SiO_2/Al_2O_3 ratio 147 (peak at −112 ppm split in to two). Our investigations are in agreement with those of other workers [7,15,16].

The ^{27}Al MAS NMR spectrum of HM and HDM (147) are depicted in Fig. 2(b). It is seen from spectrum A that there are two different environment of aluminum present in the sample. The peak at 55 ppm has been assigned to aluminum in the tetrahedral coordination present in the framework while peak near 0 ppm has been assigned to aluminum in octahedral (non-framework) environment [7,17]. After dealumination aluminum from the framework can be removed as an octahedral soluble species. This is further confirmed by decrease in peak intensity at 0 ppm for the sample with the SiO_2/Al_2O_3 ratio 147.

Fig. 3(a) shows the TGA curves of dealuminated mordenite. It is seen that T_{max} (temperature corresponding to maximum endotherm) continuously decreased with progressive Al extraction from the zeolite framework. The reduction in T_{max} can be attributed to the reduction in the number of sodium ion causing faster dehydration of the zeolite [18]. It is also clear that none of these samples exhibit an exothermic peak up to 1000 °C due to structural collapse indicating high thermal stability. Fig. 3(b) shows the TG curves for PHM zeolites. Assuming that one molecule of water is liberated by the dehydration of two hydroxyl groups, an attempt has been made to calculate the number of surface hydroxyl groups/u.c. of the impregnated samples in the temperature range of 400–750 °C from the TGA curves of PHM zeolites [19]. The values obtained are shown in Table 5. A reduction in the concentration of hydroxyl groups/u.c. of the impregnated samples indicates that some of the surface hydroxyl groups are eliminated by incorporation of phosphorous and the extent of elimination increased with the amount of impregnating material. It is suggested that elemental phosphorous binds the zeolite frame-

Table 5
Thermogravimetric data of HM and PHM zeolites (wt.% loss in different temperature range and hydroxyl groups/u.c.)

Zeolite	Total weight loss (%)	Dehydration up to 400 °C	Dehydration (750–400 °C)	Number of hydroxyl groups/u.c.
HM (13)	12.86	11.83	1.03	3.31
PHM (0.32)	11.64	10.66	0.98	3.15
PHM (0.64)	12.10	11.18	0.90	2.92
PHM (1.0)	12.49	11.66	0.83	2.70

work through oxygen causing reduction in acidic sites [20] as indicated below:

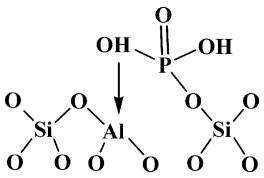

Sorption of water, *n*-hexane, cyclohexane and cumene (isopropylbenzene) over HM and HDM are shown in Table 2. The adsorption properties of mordenite depend upon the SiO_2/Al_2O_3 ratio. With increase in the SiO_2/Al_2O_3 ratio the water adsorption decreased, while there is a marginal increase in the sorption of benzene, cyclohexane and cumene [21]. A continuous increase in the *n*-hexane sorption capacity shows that *n*-hexane has access to more surface than either benzene or cyclohexane. This can also be explained on the basis of molecular size and *n*-hexane also enters those cavities that occur periodically along the walls of the main adsorption channels. From the sorption data of PHM zeolites (described in Table 6), it is seen that there is a decrease in an equilibrium capacity for hydrocarbon molecules as a result of reduction in effective pore volume due to increase in phosphorous (P) loading. *n*-Butylamine gives an estimation of the acid sites present in the solid catalysts like zeolites [22,23]. The sorption capacity for *n*-butylamine was also found to decrease with increasing amount of phosphorous loaded. This could be due to increase in concentration of POH groups of phosphorous species covering bridging hydroxyl groups [20]. From the acidity data of PHM zeolites (Table 4), it is reasonable to state that a reduction in total acidity (as accessible to NH_3 molecules) is in correlation with the percentage of phosphorous doping and is can be considered as a measure of number of acid sites covered due to modifier species.

The bulk analysis and MAS NMR study also confirmed the dealumination of HM with retention of mordenite structure (as evidenced by XRD) [7,8,24,25]. Aluminum content by chemical analysis is always higher. This difference is discussed in detail by Meyers et al. [7]. It is observed from Table 3 that stronger acidity obtained at the high-temperature desorption peak is around 36% (for HM) and varies with variation in the SiO_2/Al_2O_3 ratio in the dealuminated mordenite. This difference is noticeable in HM and HDM zeolites, related to the presence of extra-lattice Al in the HM mordenite.

Table 6
Equilibrium sorption data (mmol/g) for HM and PHM zeolites

Zeolite	HM (13)	PHM (0.32)	PHM (0.64)	PHM (1.0)
n-Hexane	0.85	0.75	0.79	0.61
Benzene	1.24	1.05	0.93	0.73
Cumene	0.38	0.44	0.39	0.31
n-Propylbenzene	0.49	0.52	0.46	0.36
n-Butylamine	1.58	1.51	1.27	1.18
Void vol. (cm^3/g)	0.1082	0.0962	0.0927	0.0903

Sorption measurement is at $P/P_0 = 0.5$ and at 25 °C. Sorption of *n*-butylamine at $P/P_0 = 0.8$ and at 25 °C.

Unlike in HZSM-5 zeolite we observed only two desorption peak maxima for mordenite in TPD of NH_3 [9,10]. We consider the peak maximum in the range of 113–122 °C (386–395 K) is due to weak and medium acid sites and the peak maximum in the range of 425–548 °C (698–821 K) is due strong acid sites. The % of stronger acid sites decreased from 36.4% to 10.5% with increasing SiO_2/Al_2O_3 ratio from 13 to 147 (Table 3).

The number of surface hydroxyl groups per unit cell was calculated from the TGA curves of PHM in the temperature range 400–750 °C (Table 5). A reduction in the concentration of surface hydroxyl groups/u.c. of the impregnated samples indicated that some of the surface hydroxyl groups are eliminated by incorporation of phosphorous. The extent of elimination increased with increased amount of incorporated material. This phenomenon resulted in the coverage of acid sites due to modifier species [19]. This is also reflected in the reduction in total acidity (as accessible to NH_3 molecules) from TPD (NH_3 desorption) as shown in Table 4. From the sorption measurement of water on HM and HDM zeolites it is inferred that the zeolite became hydrophobic on dealumination [26]. The decrease in sorption capacities with progressive increase in the incorporation of phosphorous indicated the penetration of modifier species into the zeolite channel and blocking the pores partially [20].

3.2. Catalytic degradation of EPSW

The degradation products of EPSW were oil, coke, residue and gases. The composition of oil mainly included styrene monomer (SM). The styrene dimer (SD), benzene (B), toluene (T), ethylbenzene (EB), isopropylbenzene (IPB), α-methylstyrene (α-MS), and 1,3-diphenylpropane (DPP). The heavier fractions were termed other aromatics (OT). Table 7(a) and (b) shows the product distribution and composition of oil obtained on thermal degradation (without catalyst). Table 8 indicates the PS conversion, SM selectivity, SM/SD and SM/EB molar ratios in thermal degradation. From Table 8 it can be seen that the PS conversion is linearly increased with rise in temperature. The oil yield (one of the degradation components of EPSW) increased with increase in temperature. The absence of ethylbenzene in the obtained oil is preferred on account of commercial acceptability of the process of EPSW degradation. On the basis of PS conversion, SM selectivity and SM/EB ratio, it appears that 400 °C is the optimum temperature for non-catalytic PS degradation. Table 9(a) and (b) show PS degradation products over HM and HDM zeolites along with product from thermal degradation at 360 °C. Accordingly, the catalytic performance calculated from this data is shown in Table 10. HM zeolite showed comparable SM selectivity and a slightly improved SM/SD ratio due to its acidic nature. The SM/SD ratio was in the order of HDM (86) > HM > HDM (147). The higher SM/SD ratio of HDM (86) could be ascribed to its medium acid sites density (Table 3). The results of catalytic degradation at 400 °C are

Table 7
Thermal degradation of EPSW

	Temperature (°C)			
	350	375	400	425
(a) Product distribution (wt.%)				
Oil	50.5	71.0	82.0	83.5
Coke	1.0	1.1	1.3	2.3
Residue	35.0	14.9	6.3	5.9
Balance (gaseous)	13.5	13.0	10.4	8.3
(b) Composition of oil (wt.%)				
SM	62.7	63.9	64.7	61.0
SD	1.2	4.1	5.8	6.6
B	0.1	0.1	0.1	0.1
T	6.4	4.9	4.5	4.4
EB	5.5	3.0	2.6	2.7
IPB	1.0	0.4	0.3	0.3
α-MS	13.1	7.7	6.1	6.0
DPP	2.1	5.2	4.7	5.0
OT	7.9	10.7	11.2	13.9

SM: styrene; SD: styrene dimmer; B: benzene; T: toluene, EB: ethylbenzene; IPB: isopropylbenzene; α-MS: α-methylstyrene; DPP: 1,3-diphenylpropane, OT: other aromatics.

Table 8
Characteristics of EPSW degradation (thermal degradation)

Temperature (°C)	PS conversion (%)	SM selectivity (%)	SM yield (%)	SM/SD mole ratio	SM/EB mole ratio
350	64	49.5	31.7	104.5	11.6
375	84	54.0	45.4	31.2	21.7
400	92.4	64.7	53.1	22.3	25.4
425	91.8	55.5	50.9	16.2	23.0

shown in Table 11. Nearly the same conversion as that of thermal degradation indicates that at higher temperature the catalytic degradation behaves as thermal degradation. At 400 °C, the HDM (86) showed improved SM selectivity and yield

Table 9
EPSW degradation over HM and HDM zeolites at 360 °C

Catalyst	Thermal	HM (13)	HDM (86)	HDM (147)
(a) Product distribution (wt.%) (catalyst = 1 wt.%)				
Oil	61.0	61.50	50.50	59.0
Coke	1.74	3.47	3.26	2.98
Residue	16.0	19.40	24.20	18.30
Balance (gaseous)	20.56	15.63	22.04	19.22
(b) Composition of oil (wt.%)				
B	0.06	0.07	0.06	0.06
T	5.82	6.49	6.17	5.72
EB	4.01	4.85	4.32	4.23
SM	67.36	64.21	66.94	67.71
IPB	0.59	0.73	0.63	0.60
α-MS	11.39	11.30	11.64	11.53
DPP	1.90	3.22	2.06	2.60
SD	0.92	0.86	0.61	0.93
OT	7.87	8.26	7.57	6.62

SM: styrene; SD: styrene dimmer; B: benzene; T: toluene; EB: ethylbenzene; IPB: isopropylbenzene; α-MS: α-methylstyrene; DPP: 1,3-diphenylpropane; OT: other aromatics.

Table 10
Catalytic performance of EPSW over HM and HDM zeolites at 360 °C (catalyst = 1 wt.%)

Catalyst	Thermal	HM (13)	HDM (86)	HDM (147)
SD (wt.%)	0.92	0.86	0.61	0.93
OT (wt.%)	7.87	8.26	7.57	6.62
SD + OT (wt.%)	8.79	9.12	8.18	7.55
SM/SD	146.4	149.6	219.5	145.6
SM/EB	17.2	13.5	15.8	16.3
PS conversion (wt.%)	81.6	77.1	72.5	78.2
SM selectivity (wt.%)	50.4	51.2	46.6	51.1
SM yield (wt.%)	41.1	39.5	33.8	39.9

(with no substantial difference in SM/EB ratio) compared to the corresponding values of thermal degradation which again can be ascribed to its medium acid site density. The decrease in the SM/SD ratio with increasing SiO_2/Al_2O_3 ratio is attributed to decrease in reduction in stronger acid sites on dealumination of mordenite. It can be seen that the presence of HM in the reactant mixture decreased SD + OT (from 17.0 for thermal degradation to 15.9 for HM and increased SM/SD (from 22.3 for thermal degradation to 32.1 for HM). However, on dealuminated HDM (86) and HDM (147) the reverse trend is observed for SD + OT and SM/SD mole ratios when compared with that of HM. This indicates that cracking activity of mordenite is governed by acid site density. The HDM (86) showed higher SM selectivity and yield than thermal activation, HM and HDM (147) mordenite zeolites at 400 °C. This means that medium acid site distribution in HDM (86) facilitated PS degradation selectively into SM. The acid site distribution shown in Table 3 indicates that the total acidity of HDM (86) and % strong acid sites lies intermediate between HM and HDM (147). Although overall oil yield is important, the amount of styrene in the obtained oil is also important. Therefore we assigned the SM/SD mole ratio as a measure of quality of oil.

It is widely accepted that incorporated phosphorous species binds the zeolite framework concomitantly blocking the acid sites (as shown previously) [20]. The PHM (0.32 wt.%) showed an increased SM/SD ratio with improved SM selectivity by about 6%. SM/SD ratio is also increased (185.3) by a factor of 1.27 than thermal degradation (146.4) as shown in Table 12. The PS degradation at 400 °C over phosphorous modified mordenite is demonstrated in Table 13.

Table 11
Catalytic performance of EPSW over HM and HDM zeolites at 400 °C (catalyst = 1 wt.%)

Catalyst	Thermal	HM (13)	HDM (86)	HDM (147)
SD (wt.%)	5.8	3.9	6.0	7.0
OT (wt.%)	11.2	12.0	14.0	20.8
SD + OT (wt.%)	17.0	15.9	20.0	27.8
SM/SD	22.3	32.1	21.8	16.5
SM/EB	25.4	19.3	33.3	29.4
PS conversion (wt.%)	92.4	95.7	96.7	96.4
SM selectivity (wt.%)	64.7	56.0	62.0	54.6
SM yield (wt.%)	53.1	53.6	59.9	52.2

Table 12
Catalytic performance of EPSW degradation over HM and PHM zeolites at 360 °C (catalyst = 1 wt.%)

Catalyst	Thermal	HM (13)	PHM (0.32)	PHM (0.64)	PHM (1.0)
SD (wt.%)	0.9	0.86	0.74	0.80	1.47
OT (wt.%)	7.87	8.26	6.43	6.61	7.03
SD + OT (wt.%)	8.79	9.12	7.17	7.41	8.50
SM/SD	146.4	149.6	185.3	164.1	90.4
SM/EB	17.2	13.5	16.6	14.6	15.9
PS conversion (wt.%)	81.6	77.1	73.7	76.6	78.6
SM selectivity (wt.%)	50.4	51.2	55.8	55.3	53.3
SM yield (wt.%)	41.1	39.5	41.1	42.3	41.9

Table 13
Catalytic performance of EPSW degradation over HM and PHM zeolites at 400 °C

Catalyst	Thermal	HM (13)	PHM (0.32)	PHM (0.64)	PHM (1.0)
SD (wt.%)	5.8	3.9	5.6	5.8	5.2
OT (wt.%)	11.2	12.0	13.3	16.1	13.1
SD + OT (wt.%)	17.0	15.9	18.9	21.9	18.3
SM/SD	22.3	32.1	23.0	21.7	24.8
SM/EB	25.4	19.3	28.5	32.1	26.3
PS conversion (wt.%)	92.4	95.7	96.4	96.3	96.3
SM selectivity (wt.%)	64.7	56.0	60.1	60.1	61.0
SM yield (wt.%)	53.1	53.6	58.0	57.9	58.7

Phosphorous mordenite (PHM) showed behavior similar to that of dealuminated mordenite when compared with thermal degradation of EPSW. In general the phosphorous modified zeolites showed higher SM yield and selectivity than thermal degradation (by ≈5%). The observed SM/EB molar ratio in the thermal degradation at 400 °C was 25.4 which was decreased to 19.3 in the presence of HM. This means that the SM produced on PS degradation got reduced to EB due to further hydrogenation by HM due to high acid sites density (mostly Brönsted type) associated with it. On doping 0.32 wt.% P and 0.64 wt.% P on HM, the SM/EB ratio was increased. This is attributable to the reduction in available acid site density of HM due to doping of 'P' which consequently lowered the reduction of styrene to EB. However, at 1 wt.% 'P' doping the SM/EB was lower than that observed on 0.64 wt.% P doping. This could be due to spaciousness factor (less void-space available as a result of complex formation) at relatively high metal loading. This means that the diminution of pore volume due to higher metal loading results in decreased chances to stay in pore for further cracking to lighter gaseous products. We believe that the initiation of PS degradation takes place at the external surface or at pore margins of the catalysts since PS is too large to diffuse into internal sites. The decomposed fragments of the appropriate sizes on the end bodies of the fragments will then diffuse into the zeolite pore where further cracking occurs. The modification of HM by removal of surface hydroxyl groups (the source of Brönsted acid sites) by acid leaching and masking of acid sites by metal loading invariably affects these phenomenon of PS degradation leading to SM depending on severity of the treatment of the parent zeolite (HM). Such behavior of acid treatment on variation of Brönsted acidity and its performance in polymer degradation using zeolite (clinoptilolite) has been observed by other workers [27–29]. The effect of metal loading on variation of acid sites and its correlation with catalytic performance is reported for HZSM-5 zeolites elsewhere [30]. In the present study, we have observed similar behavior by dealumination and phosphorous doping on mordenite and its effect on acidity and acid sites variation affecting catalytic performance in EPSW degradation.

The cracking of hydrocarbon on solid acids has been explained in terms of β-scission of C–C bonds [4]. The styrene monomer and dimer were probably produced by β-scission of C–C bonds in the PS main chain as follows:

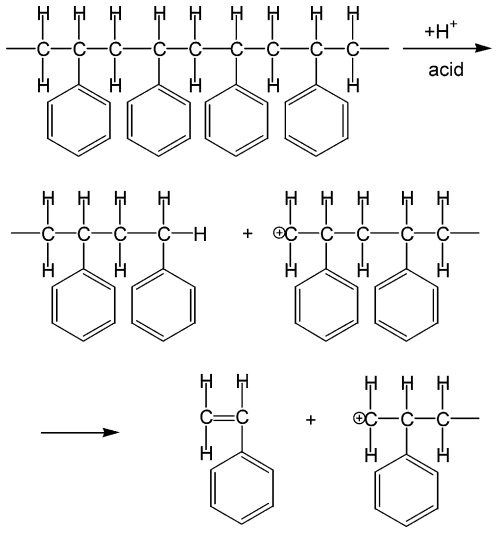

In the present work the lower yields of styrene obtained on solid acids (HM and HDM catalysts) than those obtained on simple thermal degradation (at 360 °C) are probably due to further cracking of styrene into toluene and benzene and fur-

ther hydrogenation into ethylbenzene (Tables 9 and 10). Coke formation caused by the strong interaction between acid sites and styrene or its precursors is also responsible for the lower yields of styrene on solid acids. Our results obtained at 360 °C (633 K) for PS degradation over HM and dealuminated mordenites well agreed with those reported by other researchers at 623 K [27]. The catalytic cracking of PS proceed through a complex combination of different reactions involving radical mechanism, based on chain reaction concepts, embodies elementary steps of initiation, propagation and depropagation, H-abstraction and termination [31,32]. It is reported that the benzene and ethylbenzene were produced by catalytic degradation over the solid acids [4]. This is probably because of the further cracking and hydrogenation of styrene produced, which resulted in a decrease in the fraction of styrene in the oil produced. The formation of indan derivatives on solid acids starts with an attack of a proton on the branched phenyl group to produce π-complex cation. This is then converted into σ-complex cation which is subsequently released as benzene as follows [33]:

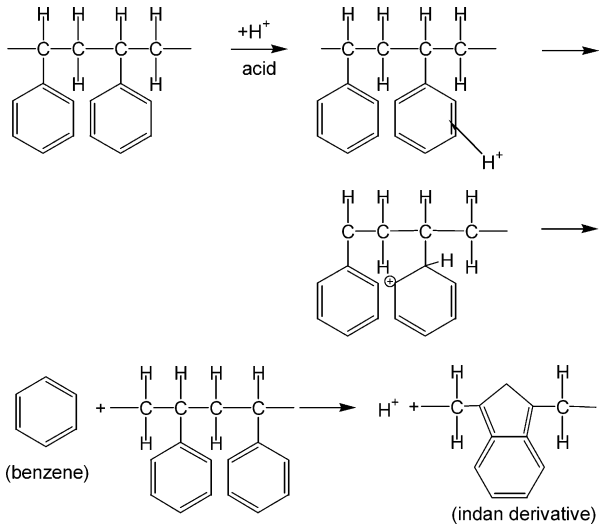

However, in the product distribution of oil obtained we did not notice the indan derivative, which is probably due to insufficient quantity which could not be detected by the column employed.

4. Conclusions

Dealumination by acid leaching of synthetic mordenite increases silica-to-alumina ratio without loss of framework structure. Dealumination reduces both weak and strong acid sites. The *ortho*-phosphoric acid impregnation reduces acid sites of HM due to binding of elemental phosphorous with zeolite framework through oxygen with diminution of pore volume. The catalytic degradation of EPSW over mordenite and modified mordenite resulted in the differences in polystyrene conversion and oil yield. The reduction in acidity of H-mordenite by dealumination and metal impregnation led to improved styrene monomer selectivity and yield when compared with thermal degradation at identical experimental conditions.

References

[1] H.S. Joo, J.A. Gain, Fuel Process. Technol. 57 (1998) 25.
[2] D.P. Serrano, J. Aguado, J.M. Escola, Appl. Catal. B 25 (2000) 181.
[3] S.Y. Lee, J.H. Yoon, J.R. Kim, D.W. Park, Poly. Degrad. Stab. 74 (2001) 297.
[4] Z. Zhang, T. Hiroshe, S. Nishio, Y. Morioka, N. Azuma, A. Ueno, H. Ohkita, M. Okada, Ind. Eng. Chem. Res. 34 (1995) 4514.
[5] W.M. Meir, D.H. Olson, Atlas of Zeolite Structure Types, Butterworths, London, 1987.
[6] P.E. Pickert, A.P. Botton, M.A. Lanewala, Chem. Eng. 75 (1968) 133.
[7] B.L. Meyers, J.H. Fleisch, G.J. Ray, J.T. Miller, J.B. Hall, J. Catal. 110 (1988) 82.
[8] M. Sawa, M. Niwa, Y. Murakami, Appl. Catal. 53 (1989) 169.
[9] N.Y. Topsoe, K. Pederson, E.G. Derouane, J. Catal. 70 (1981) 41.
[10] G.P. Babu, S.G. Hegde, S.B. Kulkarni, P. Ratnasamy, J. Catal. 81 (1983) 471.
[11] J.S. Kim, W.Y. Lee, S.B. Lee, S.B. Kim, M.J. Choi, Catal. Today 87 (2003) 59.
[12] L.B. Sand, Molecular Sieves, Soc. Chem. Ind, London, 1968.
[13] P.K. Bajpai, M.S. Rao, Ind. Eng. Chem. Prod. Res. Dev. 17 (1978) 223.
[14] R.M. Barrer, E.V.T. Murphy, J. Chem. Soc. (A) Inorg. Phys. Theor. 2506 (1970).
[15] P. Bodart, J.B. Nagy, G. Debras, Z. Gabelica, P.A. Jacobs, J. Phys. Chem. 90 (1986) 5183.
[16] G.R. Hays, W.A. Van Erp, N.C.M. Alma, P.A. Couperus, R. Husi, A.E. Wilson, Zeolites 4 (1984) 377.
[17] C.A. Fyfe, G.C. Gobbi, J.S. Hartman, J. Klinowski, J.M. Thomas, J. Phys. Chem. 86 (1982) 1247.
[18] A.J. Chandwadkar, S.B. Kulkarni, J. Thermal Anal. 19 (1980) 313.
[19] P.A. Jacobs, Carboniogenic Activity of Zeolites, Elsewhere Scientific Publ. Co., UK, 1977.
[20] W.W. Kaeding, L.B. Young, C.C. Chu, B. Weinstein, S.A. Butter, J. Catal. 67 (1981) 159.
[21] K. Itabashi, R. Fukashima, K. Igawa, Zeolites 6 (1986) 30.
[22] S.P. Mirajkar, A. Thangraj, V.P. Shiralkar, J. Phys. Chem. 94 (1990) 8589.
[23] G.N. Rao, P.N. Joshi, A.N. Kotasthane, V.P. Shiralkar, J. Phys. Chem. 94 (1992) 3073.
[24] G.E. Engelhardt, U. Lohse, A. Samoson, M. Maegi, M. Tarmak, E. Lippma, Zeolites 2 (1982) 59.
[25] T.J. Rocha, S.W. Carr, J. Klinowski, Chem. Phys. Lett. 187 (1991) 401.
[26] N.Y. Chen, J. Phys. Chem. 80 (1976) 60.
[27] J.R. Kim, Y.A. Kim, J.H. Yoon, D.W. Park, H.C. Woo, Poly. Degrad. Stab. 75 (2002) 287.
[28] E.Y. Hwang, J.K. Choi, D.H. Kim, D.W. Park, H.C. Woo, Korean J. Chem. Eng. 15 (1998) 434.
[29] D.W. Park, E.Y. Hwang, J.R. Kim, J.K. Choi, Y.A. Kim, H.C. Woo, Poly. Degrad. Stab. 65 (1999) 193.
[30] K.H. Chandavar, S.G. Hegde, S.B. Kulkarni, P. Ratnasamy, J. Chem. Tech. Biotechnol. 34 (1984) 165.
[31] G. De la Puente, J.M. Arandes, U.A. Sedran, Ind. Eng. Chem. Res. 36 (1997) 4530.
[32] H. Nanbu, Y. Sakuma, Y. Ishihara, T. Takesue, T. Ikemura, Poly. Degrad. Stab. 19 (1987) 61.
[33] H. Ukei, T. Hiroshe, S. Horikawa, Y. Taka, N. Azuma, A. Ueno, Catal. Today 62 (2000) 67.